Int. J. Multiphase Flow Vol. 19, No. 6, pp. 1013–1027, 1993
Printed in Great Britain. All rights reserved

0301-9322/93 $6.00 + 0.00
Copyright © 1993 Pergamon Press Ltd

FLOW OF A THIN FILM OVER A PERIODIC SURFACE

S. SHETTY and R. L. CERRO†
Chemical Engineering Department, University of Tulsa, Tulsa, OK 74104, U.S.A.

(Received 1 August 1992; in revised form 10 October 1993)

Abstract—The flow of thin viscous films over complex surfaces is relevant to the description of heat and mass transfer processes in ordered packing materials. Ordered packings, usually made of corrugated sheets of metal, plastic or ceramic materials have important operating advantages and usually outperform random packings of similar characteristics. A two-dimensional streamline function is used to compute the components of the velocity field and to reduce the equations of motion to a single, nonlinear, ordinary differential equation for the film thickness. A perturbation solution for small film thickness is developed that predicts two film surface maxima for each cycle of the solid surface. Normal film thickness profiles are measured in a direction normal to the solid surface, as opposed to experimental film thickness measured in a direction normal to the axis of the solid surface. The agreement between experimental and theoretical normal film thickness is very good for small values of the parameter δ, defined as the ratio of the Nusselt film thickness and the amplitude of the wavy solid surface.

Key Words: viscous film flow, periodic surface, packings

1. INTRODUCTION

The flow of a liquid film down an inclined plane is important in many chemical engineering processes, e.g. film condensation, painting, evaporation and many coating processes. There are a number of papers on the experimental and theoretical characterization of falling films, starting with the comprehensive review of Fulford (1964). Most papers, however, deal with films on smooth, flat surfaces. Few theoretical works (Wang 1981; Dassori *et al.* 1984; Pozrikidis 1988; Zhao 1991) and only one instance of experimental data (Zhao & Cerro 1992) exist on free surface flows over solid surfaces with a periodic shape. Wang (1981) studied the three-dimensional flow of a liquid over a sinusoidal surface using a perturbation analysis that was limited to small amplitudes of the wavy plate as compared to the average depth of the fluid. Wang's (1981) results are relevant for the flow of very thick films or for films over periodic surfaces of very small amplitude, i.e. micro-structures. Dassori *et al.* (1984) studied the flow of a thin film in a sinusoidally wavy channel with small-amplitude striations along with a countercurrent gas flow. Unfortunately, the choice of the cross-section thickness of the gas phase as the characteristic scaling parameter of their perturbation renders their results unsuitable for our analysis. More relevant to this study are the numerical results of Pozrikidis (1988) where a boundary-integral computational analysis of the creep-flow equations of motion is introduced, that is valid for surfaces of arbitrary geometry. Pozrikidis' (1988) computations, however, were carried out only for sinusoidal and rectangular corrugations.

Flows of viscous films over complex surfaces occur both in nature and in many chemical processes. The primary motivation for this work is the flow of liquid films over ordered packings. Ordered packings are widely used in the chemical industry in gas–liquid contacting devices. They have a well-defined structure and outperform random packings in difficult separations with pressure gradient constraints, low relative volatilities and/or small liquid holdup. Recently, de Santos *et al.* (1991) published a scholarly historical introduction and a comprehensive review of packing functionality. Ordered packings are usually made of corrugated sheets that may have been mechanically or chemically treated to improve their wetting characteristics. They have a well-defined macro- and micro-structure. The macro-structure, in the way of channel geometry generated by corrugations, configures the mixing cells for the bulk flow of the vapor phase. The

†To whom all correspondence should be addressed.

micro-structure, such as surface indentations, perforations, chemical treatment or gauze-like nature of the packing material, plays an important role in sustaining a stable, wetting liquid film.

The specific problem considered in this work is the steady flow of a viscous liquid film over a periodic surface, where the film thickness is small compared to the amplitude and wavelength of the solid surface. Thin films are conceptually interesting becuase they can be described by a simple streamline function and important in practice because they are representative of the flow over the macro-structure of commercial packings.

2. PREVIOUS EXPERIMENTAL WORK ON COMPLEX SURFACES

In the analysis of viscous films on flat surfaces an important parameter is the Nusselt film thickness h^*, presented here for a vertical surface:

$$h^* = \left(\frac{3\nu q}{g}\right)^{1/2}. \qquad [1]$$

The Nusselt film thickness is the average thickness of a film of kinematic viscosity ν, flowing at rate q on a vertical flat surface; g is the acceleration due to gravity. The Nusselt film thickness is used here as a characteristic film thickness. Zhao & Cerro (1992) obtained experimental data on film thickness and streamline patterns on S surfaces, i.e. surfaces made of a sequence of concave and convex half-circles, approaching a sine-shaped surface. Their data was taken on a brass surface of radius $r = 1.5875 \times 10^{-3}$ m (1/16″) with amplitude A equal to the radius and wavelength $a = 6.35 \times 10^{-3}$ m. The resulting amplitude/wavelength ratio was $\lambda = 0.25$. From these experiments and their own numerical computations (Zhao 1991), Zhao & Cerro (1992) concluded that three parameters are needed to correlate the experimental data: (1) the ratio of the Nusselt film thickness to the solid surface amplitude, $\delta = h^*/A$; (2) the Reynolds number, $\mathrm{Re} = q/\nu$; and (3) the Capillary number, $\mathrm{Ca} = \mu q/\sigma h^*$. These three dimensionless parameters represent the three conditions, that during experiments can be chosen independently for a given type of solid surface: (1) flow rate, (2) kinematic viscosity and (3) surface tension.

In their experiments, Zhao & Cerro (1992) analyzed values of the relative thickness parameter from $0.24 \leqslant \delta \leqslant 0.6$. For flow rates of industrial interest, this range is representative of the flow over the micro-structure of ordered packings. Zhao & Cerro (1992) observed that for larger values of δ, the free surface of the liquid film is flat and as the value of δ decreases, the free surface becomes periodic with the same wavelength as that of the solid surface. Even at their lowest experimental Reynolds numbers, inertial and capillary effects could not be neglected since streamlines had a very small radius of curvature. The experiments reported here were performed over an S surface and fall in the range $0.1 \leqslant \delta \leqslant 0.17$. These values of δ are well within the range of values that can be found in the operating range of industrial packing surfaces.

3. THEORETICAL FILM EVOLUTION

For a Cartesian coordinate system defined as shown in figure 1, the position of the solid surface is described by a periodic function of amplitude R and wavelength a. Equation [2] describes two smoothly joined half-circles centered at $x = x_c$ and $y = y_c$:

$$y_s = y_c \pm \sqrt{R^2 - (x_s - x_c)^2}. \qquad [2]$$

The tangent to the solid surface defines an angle θ, with respect to the vertical x-direction. This angle can be obtained as a function of the geometrical parameters of the solid surface:

$$\theta = \arctan\left(\frac{dy_s}{dx}\right) = \arctan\left[\frac{\pm(x_s - x_c)}{\sqrt{R^2 - (x_s - x_c)^2}}\right]. \qquad [3]$$

The physical components of gravity, i.e. the components of the vector in a Cartesian system in the directions tangential and normal to the solid surface are given as functions of θ:

$$g_s = g\cos\theta = \frac{g}{\sqrt{1 + \tan^2\theta}} \qquad [4]$$

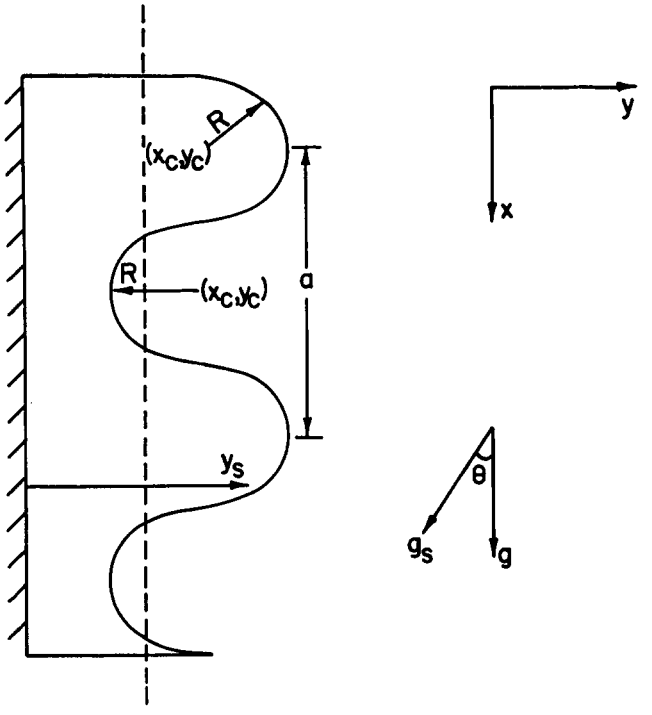

Figure 1. Sketch of the solid surface and definition of the geometric variables.

and

$$g_n = g \sin\theta = \frac{g \tan\theta}{\sqrt{1+\tan^2\theta}}. \qquad [5]$$

The physical components of gravity given by [4] and [5], are double-periodic functions, i.e. elliptic functions in the sense defined by Whittaker & Watson (1927), undergoing two periods for every period of the solid surface. Substitution of the components of gravity into the linear momentum balance equations renders a system of equations with a periodic body force. Based on a single unknown function, $h(x)$, a two-dimensional streamline function can be defined and then used to compute the physical components of the velocity vector:

$$\psi(x,y) = \frac{3q}{2}\left[\frac{y^2}{h(x)^2} - \frac{y^3}{3h(x)^3}\right], \qquad [6]$$

$$v_x = \frac{\partial\psi}{\partial y} = \frac{3q}{2h(x)}\left[2\frac{y}{h(x)} - \left(\frac{y}{h(x)}\right)^2\right] \qquad [7]$$

and

$$v_y = -\frac{\partial\psi}{\partial x} = \frac{3q}{2}\frac{dh}{dx}\left[2\frac{y^2}{h(x)^3} - \frac{y^3}{h(x)^4}\right]. \qquad [8]$$

The function $h(x)$ is the local film thickness. The components of the velocity vector given by [7] and [8] satisfy continuity, the non-slip condition at the solid surface and a simple version of the free-shear boundary condition at the free surface. Substitution of [7] and [8] into the linear momentum balance in the x-direction results in an ordinary differential equation for the local film thickness, $h(x)$. The normal stress boundary condition is introduced in order to compute the pressure at the free surface (Higgins *et al.* 1977):

$$p(x,h(x)) = -\sigma 2\mathscr{H}, \qquad [9]$$

where $2\mathscr{H}$ is the mean curvature of the free surface. In dimensionless form the resulting equation is

$$\mathrm{Re}\left(\tfrac{29}{140}\phi'^3\delta^3\lambda^3 - \tfrac{2}{5}\phi'\delta\lambda - \tfrac{29}{70}\phi\phi'\phi''\delta^3\lambda^3 + \tfrac{29}{140}\phi^2\phi'''\delta^3\lambda^3\right)$$

$$= \cos\theta\phi^3 + \frac{\cos\theta}{2}\phi^4\delta\lambda\frac{d\theta}{dX} + \sin\theta\phi^3\phi'\delta\lambda - 1 - \frac{\phi^3\delta^2\lambda}{3\,\mathrm{Ca}}\frac{d2\mathscr{H}}{dX} + \phi'^2\delta^2\lambda^2 + \phi^4\delta^4\lambda^4$$

$$-\frac{\delta^2\lambda^2}{2}\phi\phi'' - 3\phi\phi'^2\phi''\delta^2\lambda^2 + \tfrac{21}{20}\phi^2\phi''^2\delta^4\lambda^4 + \tfrac{9}{10}\phi^2\phi'\phi'''\delta^4\lambda^4 - \frac{3\delta^4\lambda^4}{20}\phi^3\phi''''. \qquad [10]$$

Equation [10] is the complete form of the film evolution equation for a free surface flow defined by the streamline function $\psi(x, y)$. The left-hand side members of [10] are the inertial terms. The first three members on the right-hand side of [10] are the body force terms. The number, 1, is the leading viscous term of the linear momentum balance in the x-direction. The term that has the Ca and the derivative of the Gaussian curvature in it, is the capillary contribution to the pressure field and the rest are the remaining viscuous terms.

There are three relevant characteristic lengths in this problem. One of the characteristic lengths is the amplitude of the solid surface, i.e. the radius of the "half-circle" surface, $A = R$. The second characteristic length is the wavelength of the solid surface, a. The ratio between the amplitude of the solid surface and the wavelength is the dimensionless wavenumber, λ. The third characteristic length is the Nusselt film thickness, h^*. The Nusselt film thickness is used as the characteristic length in the definition of the dimensionless film thickness, ϕ. Implicit is the assumption that the thickness of the viscous film on a periodic surface is of the same order of magnitude as the thickness of the film on a flat, vertical surface. The wavelength of the solid surface is used to define the dimensionless coordinate length, X. The amplitude of the solid surface, $A = R$, is used to define the dimensionless radius of curvature, i.e. the inverse of the dimensionless mean curvature, $2\mathscr{H}$. For a general periodic surface, λ and δ can be varied independently. For all the experiments reported in this work, the value of the wavenumber was constant and equal to $\lambda = 0.25$. The thickness parameter, δ, can be assumed to be a small number, $0.1 \leqslant \delta \leqslant 0.2$, such that the product of the thickness parameter and the wavenumber is very small; $0.025 \leqslant \delta\lambda \leqslant 0.050$.

A perturbation solution can be obtained by introducing a perturbation parameter ε, defined by the product of the thickness parameter and the wavenumber, $\varepsilon = \delta\lambda$. It was shown that for the range of interest of this work, ε is indeed a very small number. Rearrangement of [10] in powers of this perturbation parameter leads to a singular perturbation. For small average film thickness and large solid surface amplitude and wavelength, as was the case in this work, the film evolution equation finally reduces to the following algebraic expression:

$$\phi_0^3\left[1 - \left(\frac{x_s - x_c}{R}\right)^2\right]^{1/2} - 1 = 0, \qquad [11]$$

where

$$\left[1 - \left(\frac{x_s - x_c}{R}\right)^2\right]^{1/2} = \cos\theta; \qquad [12]$$

[11] is similar to the Nusselt solution for the flow of a liquid film over a solid surface inclined at a constant angle θ with respect to the vertical direction. Equation [11], however, applies to a thin film flowing over a periodic surface for continuously varying values of θ. The description of the flow of a viscous film over a periodic surface, can therefore be approximated by a sequence of quasi-steady state Nusselt solutions for viscous film flow over a surface of varying inclinations:

$$\phi_0(x) = \frac{1}{\left[1 - \left(\frac{x_s - x_c}{R}\right)^2\right]^{1/6}}. \qquad [13]$$

The dimensionless film thickness predicted by [13] is a remarkably simple but accurate representation of the varying thickness of thin films over a periodic surface. It will be shown that

Table 1. Parameters for the experimental data in this work (in all cases the solid surface wavelength was $a = 0.0254$ m and the fluid used was silicone oil)

q (m^3/s-m)	h^* (mm)	ρ (kg/m^3)	μ (kg/m-s)	σ (N/m)	δ	Re	Ca
5.25E − 06	0.6848	970.4	0.1941	0.0214	0.1078	0.0262	0.1043
5.91E − 06	0.7122	970.4	0.1941	0.0214	0.1122	0.0295	0.1128
8.20E − 06	0.7946	970.4	0.1941	0.0214	0.1251	0.0410	0.1404
1.00E − 05	0.8490	970.4	0.1941	0.0214	0.1337	0.0500	0.1603
1.13E − 05	0.8846	970.4	0.1941	0.0214	0.1393	0.0566	0.1741
1.31E − 05	0.0929	970.4	0.1941	0.0214	0.1464	0.0656	0.1921
1.36E − 05	0.9408	970.4	0.1941	0.0214	0.1482	0.0681	0.1969
1.43E − 05	0.9557	970.4	0.1941	0.0214	0.1505	0.0714	0.2032
1.62E − 05	0.9978	970.4	0.1941	0.0214	0.1571	0.0812	0.2214
1.74E − 05	1.021	970.4	0.1941	0.0214	0.1608	0.0869	0.2317
1.79E − 05	1.030	970.4	0.1941	0.0214	0.1622	0.0894	0.2361
1.89E − 05	1.0488	970.4	0.1941	0.0214	0.1652	0.0943	0.2531
1.98E − 05	1.0668	970.4	0.1941	0.0214	0.1679	0.0992	0.2531
2.05E − 05	1.0784	970.4	0.1941	0.0214	0.1698	0.1025	0.2587
3.44E − 05	1.0175	969.8	0.0969	0.0214	0.1602	0.3445	0.2303
3.51E − 05	1.024	969.8	0.0969	0.0214	0.1613	0.0351	0.2332

[13] agrees very well with the experimental data under conditions where capillary forces are not relevant and the relative film thickness is small.

4. EXPERIMENTAL SETUP

The amplitude of the solid surface is equal to the radius, $R = 6.35 \times 10^{-3}$ m (0.25″) and the wavelength is $a = 0.0254$ m (1″). See figure 1 for a definition of the geometric variables. The ratio of amplitude to wavelength, $\lambda = 0.25$, was identical to that of the S surface used by Zhao & Cerro (1992). The solid surface used in these experiments was made of stainless steel. Table 1 lists the flow rates, Nusselt film thickness, the thickness parameter δ and the fluid properties, as well as the Re and Ca for all experimental runs.

The experimental setup is shown schematically in figure 2. The test surface is 0.1016 m wide and 0.1016 m long. The test surface is set in a vertical position directly under the flow distributor. The narrow slit (0.001 m wide) of the flow distributor traverses the entire solid surface width to ensure a uniform liquid distribution. The liquids used in these experiments were silicone oils, of kinematic viscosity 0.1 and 0.2 St, respectively. A constant overflow overhead tank is used to maintain a constant liquid flow rate. The tank is placed about 1.5 m above the liquid distributor. A micro-pump is used to recycle the liquid back to the overhead tank. Liquid flow rates were

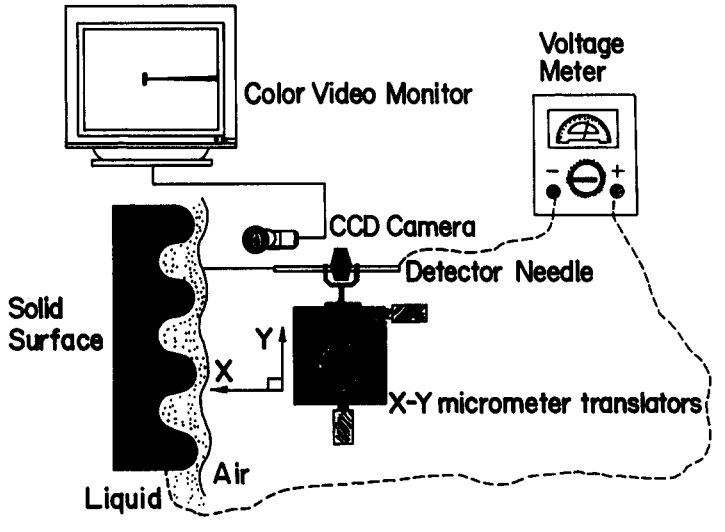

Figure 2. Sketch of the experimental apparatus.

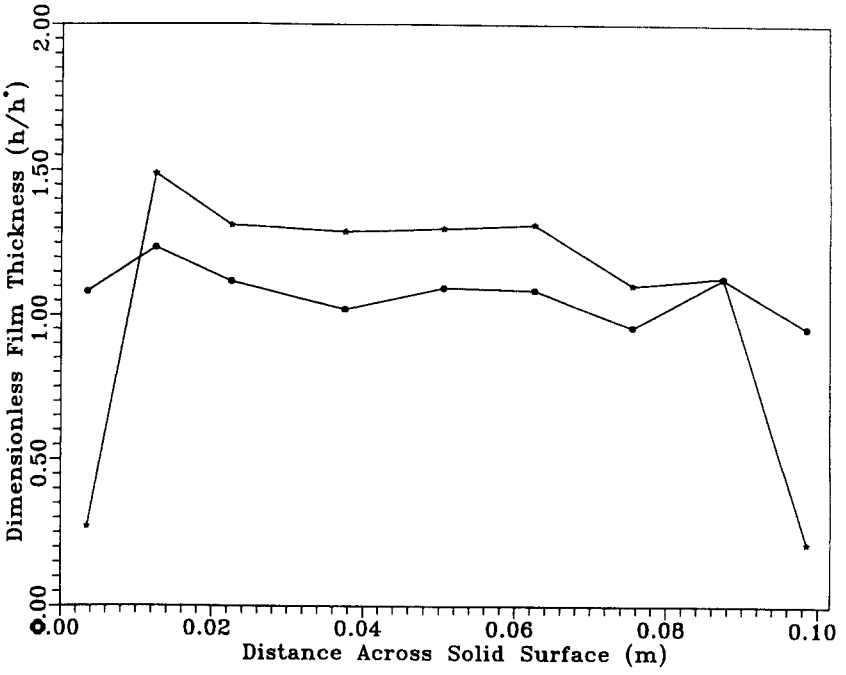

Figure 3. Liquid film distribution across the experimental solid surface, $h^* = 7.31 \times 10^{-4}$ m: ★, Position along the solid surface $x = 0.0$ m; ●, position along the solid surface $x = 0.1$ m.

measured by collecting the liquid flowing over the test surface in a graduated measuring cylinder over a known period of time. All experimental measurements were made at steady state, i.e. after a constant flow rate was achieved. A very thin needle mounted on an x–y precision micrometer translator is used to detect the position of the free surface and the solid surface. The minimum register of the x–y micrometer translators is 10^{-6} m. The translator ensemble is mounted on a vertical tubular bench with a horizontal translator that enables the needle to be placed at any point on the test surface. The entire experimental assembly is mounted on the Oriel optical table. The back of the test surface and one end of the needle are connected to a laboratory ohmmeter. Due to the large difference in electrical conductivity between the solid surface and silicone oil, it is possible to detect the position of the solid surface when the needle touches it. This causes the ohmmeter needle to deflect and the micrometer reading can be recorded to obtain the position of the solid surface. Since the conductivity of silicone oil is very low, however, the position of the free surface is detected with a combination of side-lighting and a video-camera zoomed in on the liquid surface to detect the location at which the needle first touches the free surface. The micrometer reading then, indicates the position of the free surface. In a typical measurement, the needle is originally away from the liquid surface. As the needle moves forward, the position of the free surface is determined by the change in the free surface detected by the enhanced video image. The needle then moves forward until it touches the solid surface. This position is detected by the deflection of the conductivity meter. While it is not practially possible to align the test surface absolutely parallel to the tubular bench carrying the x–y translators, the error in the position of two consecutive solid surface maxima was found to be no greater than 0.3°. By repeating the procedure described above at any experimental position, several times, it was determined that the average deviation in the location of either the free surface or solid surface was always smaller than 10^{-5} m.

Film thickness profiles obtained across the width of the solid surface, were used to verify that the film was uniformly distributed across the test surface. The film thickness measurements shown in figure 3 were made across the width of the solid surface at two different x-locations. One of the measurements was done at a valley of the solid surface and one at a peak. The edge effects are seen only in narrow strips on either side of the test structure. The corrections to be made in the liquid flow rate per unit width to account for these edge effects are $< 5\%$ of the total flow rate. Film thickness measurements along the length of the solid surface, over a length of one period,

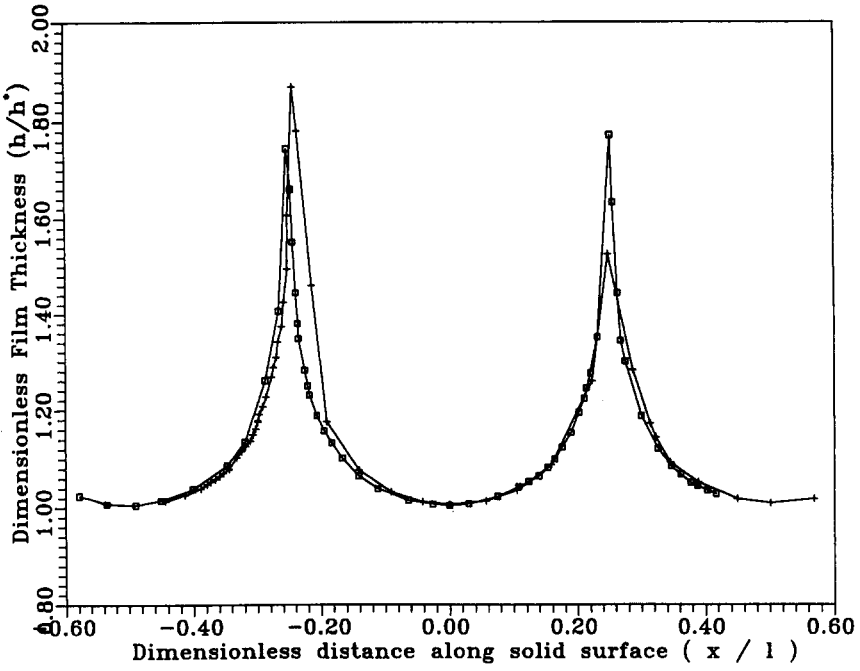

Figure 4. Repeatability of normal film thickness data; $h^* = 9.97 \times 10^{-4}$ m.

were also performed at three difference locations, located 0.023, 0.053 and 0.074 m, respectively, from the left edge of the solid surface. The average deviation in film thickness across this width was close to 10%. Repeatability of experimental data was also verified by comparing similar experimental runs performed on two different occasions. Figure 4 shows two such experimental determinations. The average deviation between the two film thickness profiles was $< 5\%$, indicating agreement compatible with experimental error.

5. CALCULATION OF NORMAL FILM THICKNESS

Film thicknesses were measured experimentally by moving the needle in the direction y, normal to the direction of flow. Figure 5 shows the position of the solid surface and the free surface for a typical experimental run. The film thickness in a fixed coordinate system shown in figure 5 is the difference between the y-position of the free surface and the y-position of the solid surface. The theoretical film thickness, developed for a convective coordinate system and described by [13] is measured in a direction **normal** to the solid surface. In the development of the perturbation solution, it was assumed that the thickness of the film is of the same order of magnitude as the thickness of a film on a flat vertical surface and that the film thickness is many times smaller than the radius of curvature of the solid surface.

For a correct comparison of experimental and theoretical film thickness profiles, it is therefore necessary to calculate the experimental film thickness normal to the solid surface at every point. Since the test surface is made of a collection of "half-circle" surfaces, the normal to the surface must pass through the center of the circle. A geometrical construction can be used to transform the film thickness measured experimentally in the direction normal to the axis of the solid surface into the film thickness measured normal to the local tangent of the solid surface. The geometrical variables are defined in figure 6.

Assume that the solid surface and the liquid free surface can be described by two continuous functions of the position along the direction of flow, $f(x)$ and $g(x)$ respectively. The set of N experimental points along the solid surface can be described as a set $x(i)$ and $f(x(i))$, for $i = 1, \ldots, N$. Each of these points have a unique corresponding point at the liquid free surface denoted by $x_r(i)$, $g_r(x(i))$. Notice that the free surface position in the normal direction corresponds to the position $x_s(i)$ of the solid surface, not the position $x_r(i)$ of the liquid free surface. The set

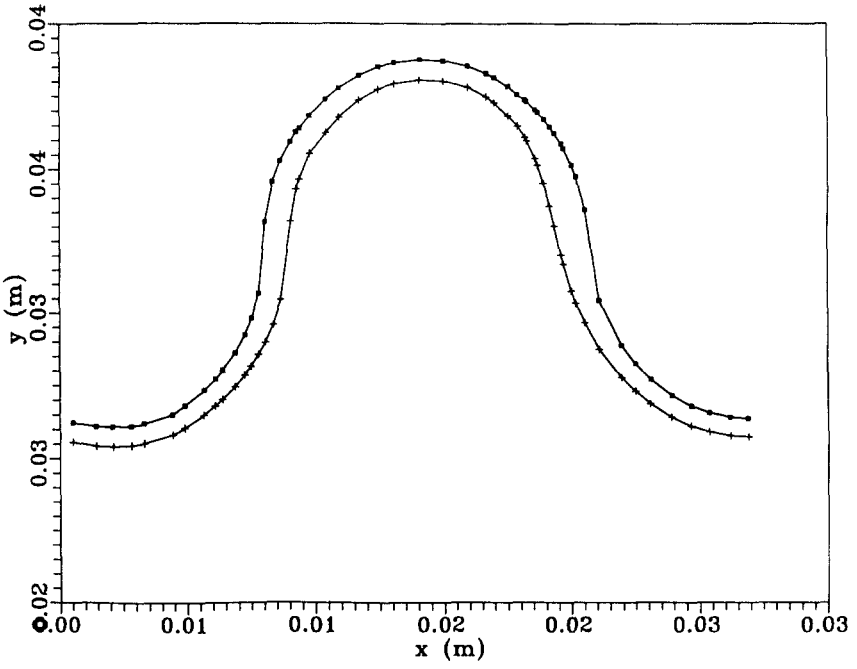

Figure 5. Typical experimental data for film thickness measurement. Silicone oil (200 St), $q = 5.25 \times 10^{-6}$ m^3/s-m, $h^* = 6.85 \times 10^{-4}$ m: ■, solid surface; +, free surface.

of coordinates, $x(i)$, $f(x(i)$ and $g_r(x(i))$ determines the position of the solid and free surfaces at the position $x(i)$ along the direction of flow.

The first step in the execution of the algorithm consists of guessing the position of the interval along the free surface intersected by the normal to the solid surface. The normal to the solid surface passes through the center of the circle, $[x_c, y_c]$, and through the point at the solid surface. The slope of the normal is given by

$$m_1 = \frac{f(i) - y_c}{x(i) - x_c}. \qquad [14]$$

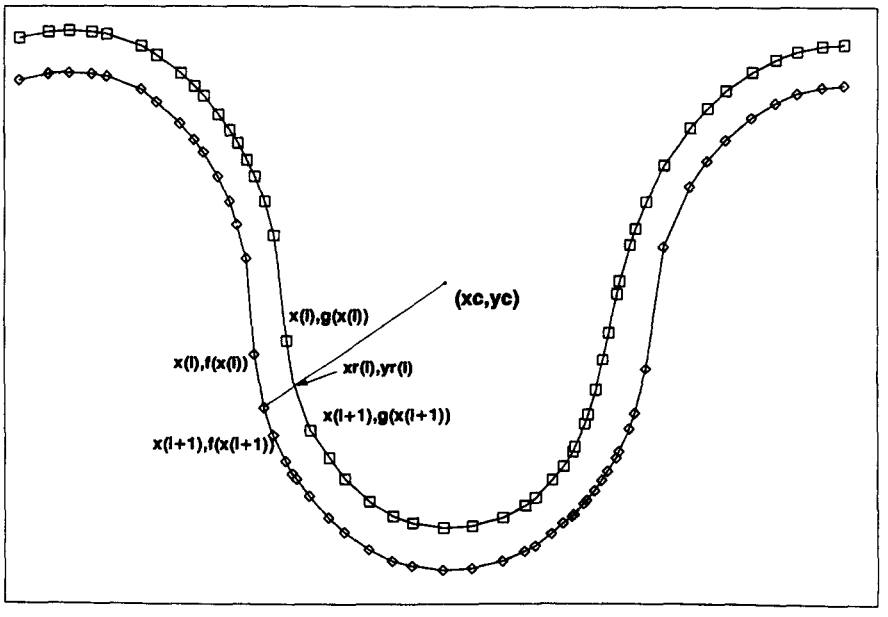

Figure 6. Geometric variables needed to calculate normal film thickness: □, free surface; ◇, solid surface.

The equation for the normal passing through the points $(x(i), f(i))$ and (x_r, y_r) is then given by

$$y_r - f(i) = m_1[x_r - x(i)]. \quad [15]$$

In addition, the line joining the points at the free surface, (x_r, y_r), and the experimental points $[x(i+1), g(i+1)]$ is given by a straight line with slope

$$m_2 = \frac{y_r - g(i+1)}{x_r - x(i+1)}, \quad [16]$$

such that the corresponding equation for this line segment is given by

$$y_r - g(i+1) = m_2[x_r - x(i+1)]. \quad [17]$$

Equations [15] and [16] can be solved for x_r, after eliminating y_r, to give

$$x_r = \frac{g(i+1) - f(i) + m_2 x(i+1) + m_1 x(i)}{m_1 - m_2}. \quad [18]$$

If $x_r < x(i)$, then the guess of the position of the interval along the surface must be improved by making $i = i - 1$. If, on the other hand, $x_r > x(i+1)$, then $i = i + 1$. In both cases, the next step consists of computing a new value of x_r. With this value of x_r, the value of y_r is obtained by rational interpolation of the free surface experimental data. The film thickness normal to the solid surface at $(x(i), f(i))$ is then given by

$$h(x) = \sqrt{[x(i) - x_r]^2 + [y(i) - y_r]^2}. \quad [19]$$

Figure 7 provides a comparison between the film thickness measured normal to the axis of the solid surface and the film thickness measured normal to the solid surface at every point.

6. RESULTS AND COMMENTS

For small ratios of Nusselt film thickness to solid surface amplitude, the liquid film closely follows the changes in inclination of the solid surface and the film thickness is seen to be distinctly doubly periodic, i.e. two maxima in film thickness are observed for each period of the solid surface.

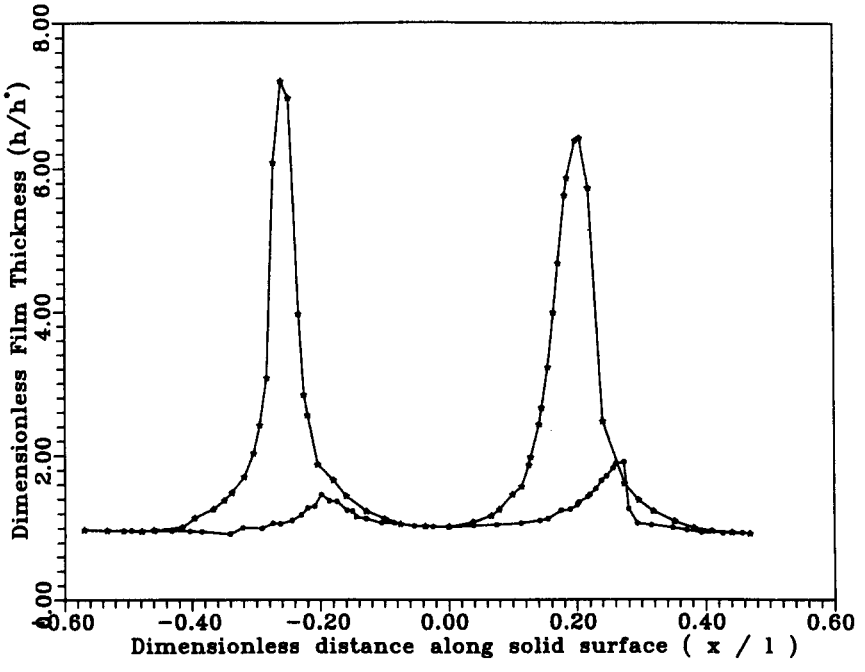

Figure 7. Comparison of film thickness data; $h^* = 6.85 \times 10^{-4}$ m: ★, laboratory coordinates. ●, normal to the solid surface.

One of the film thickness maxima is nearly always greater than the other one. An explanation of this asymmetry may be found in the effect of the gravity field normal to the flow on the pressure field. This effect is accounted for in [10] by the term that is multiplied by $\sin\theta$. Unfortunately, this term does not appear in the lower perturbation solution, [13]. In the region where $\sin\theta < 0$, the normal component of gravity will point from the solid surface to the free surface and this contribution will decrease the pressure below the free surface. On the other hand, when $\sin\theta > 0$, the normal component of gravity points from the free surface to the solid surface and this contribution will increase the pressure below the free surface. As the fluid moves over the solid surface, transition from a lower than atmospheric pressure to a higher than atmospheric pressure region, generates a pressure gradient that accelerates the film flowing over the outer surface and decelerates the film flowing over the inner surface.

Figures 8–10 compare the film thickness calculated using the low Re perturbation solution and the experimental film thickness normal to the solid surface. The values of δ are 0.108, 0.146, and 0.161, respectively. The agreement between the experimental and theoretical computed film thickness is quite good and the discrepancies between these values are within the limits of experimental error. Most striking is the coincidence of the positions of the maxima and minima of the experimental and theoretical film thickness. The normal film thickness data of Zhao & Cerro (1992), obtained on the solid surface with wavelength $= 6.35 \times 10^{-3}$ m (1/4″) were also compared with the thin film perturbation solution (figures 11 and 12). The experimental normal film thicknesses generated with this smaller surface for the concave region of the solid surface are considerably larger than the values predicted by theory. The film thickness profiles, i.e. the thickness measured along the axis of the solid surface, are single-periodic with a wavelength equal to the wavelength of the solid surface. The position of the normal film thickness peaks along the solid surface, show remarkably good agreement between theoretical and experimental values.

To highlight the role of the relative ratio of film thickness to surface amplitude, the effect of Nusselt film thickness on the normal film thickness profiles was explored for a wide range of values of δ. Figure 13 shows the normal film thickness of silicone oil for $0.083 \leqslant \delta \leqslant 0.475$. For very small values of δ, the normal film thickness profile is distinctly double-periodic with respect to the solid surface wavelength. There are two maxima of nearly equal height and the regions of minima are very close for the concave and convex sectors of the solid surface. Increasing the flow rate, and consequently the value of δ, a smooth transition occurs whereby the concave section of the solid

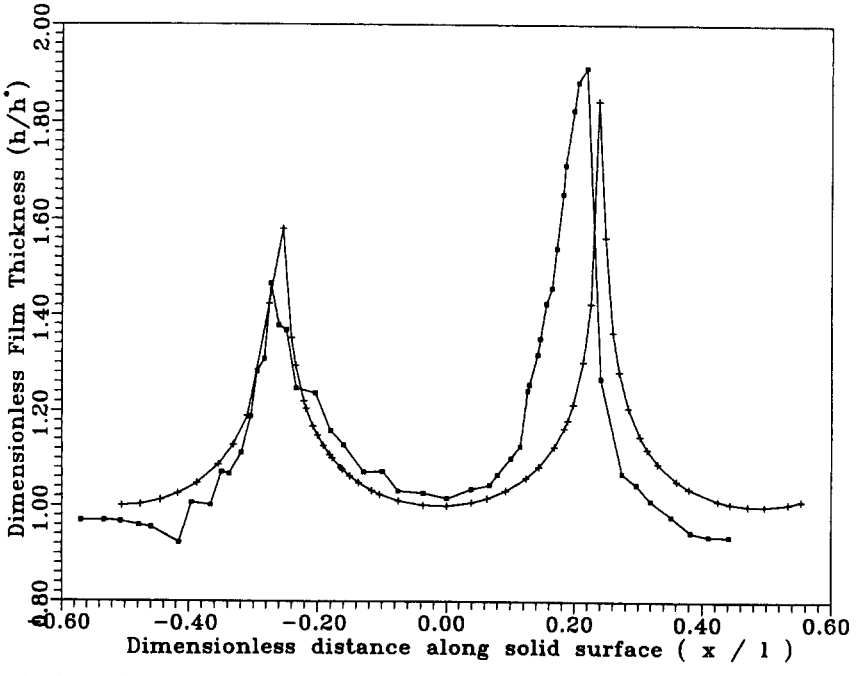

Figure 8. Comparison of experimental normal film thickness with the perturbation solution [14]; $a = 0.0254$ m, $h^* = 6.85 \times 10^{-4}$ m: ■, experimental; +, theoretical.

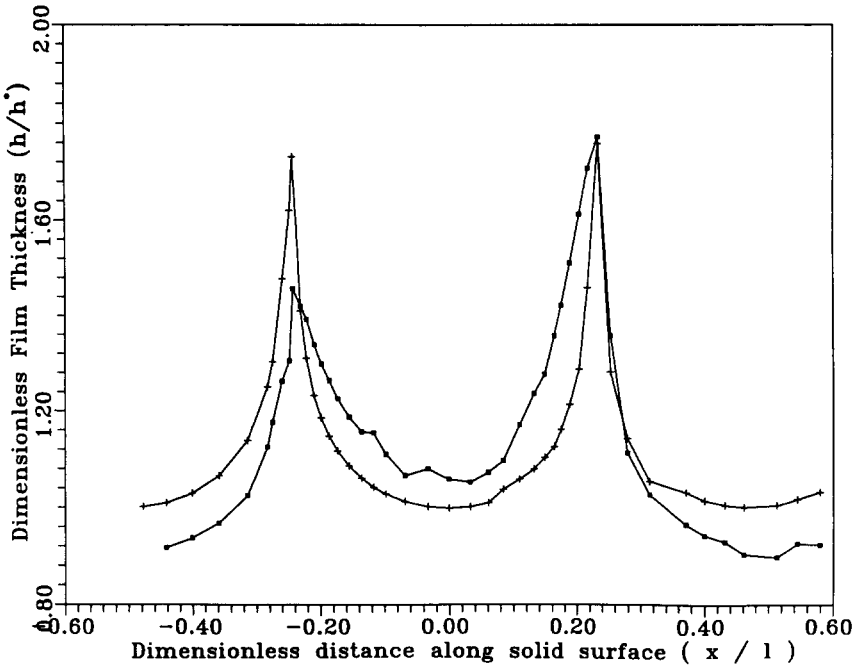

Figure 9. Comparison of experimental normal film thickness with the perturbation solution [14]; $a = 0.0254$ m, $h^* = 9.29 \times 10^{-4}$ m: ■, experimental; +, theoretical.

surface becomes increasingly filled with liquid and the overall shape of the liquid surface departs from the theoretically predicted shape. The concave sections of the solid surface are now very different from the convex section and the overall shape of the free surface is periodic with a wavelength equal to the wavelength of the solid surface.

Two other important parameters are used to correlate the experimental data: (1) the amplitude ratio of film thickness to solid surface amplitude; and (2) the phase shift. These two parameters can be defined with respect to the free surface position or with respect to the actual film thickness.

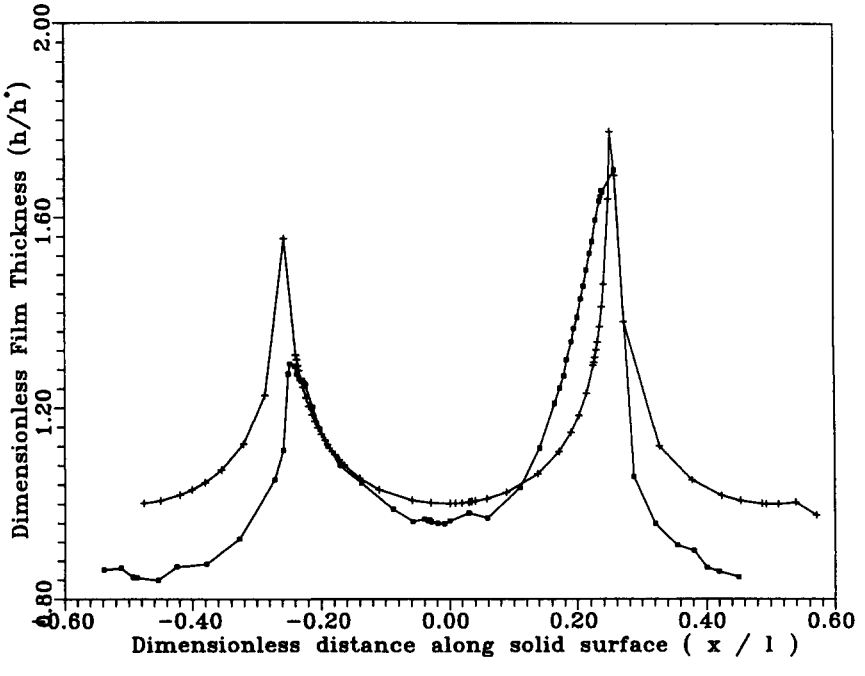

Figure 10. Comparison of experimental normal film thickness with the perturbation solution [14]; $a = 0.0254$ m, $h^* = 1.021 \times 10^{-3}$ m; ■, experimental +, theoretical.

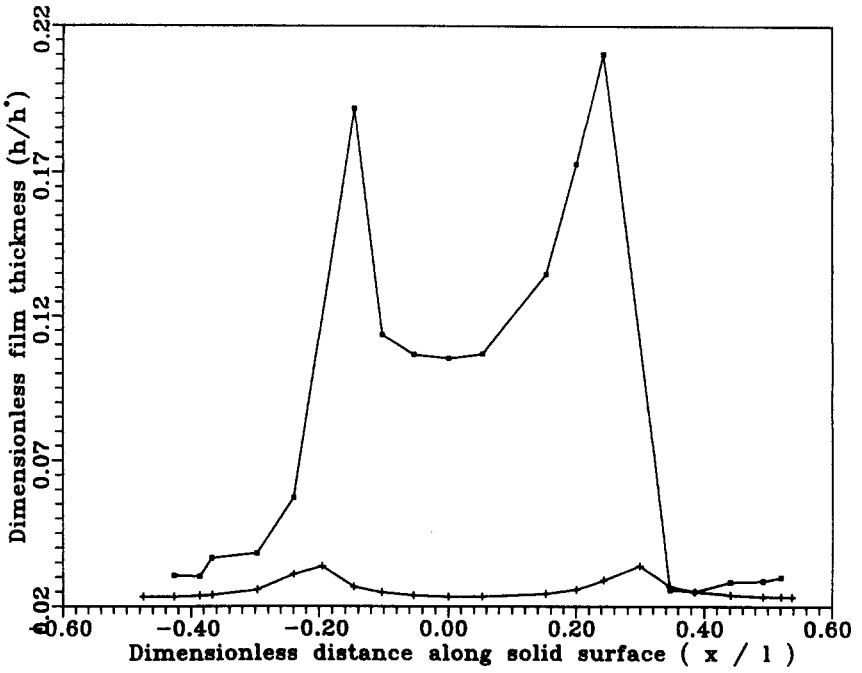

Figure 11. Comparison of experimental normal film thickness with the perturbation solution [14]; $a = 0.00635$ m, $h^* = 7.5 \times 10^{-4}$ m; ■, experimental +, theoretical.

The amplitude of the liquid film thickness is defined as one-half the difference between the maximum and the minimum thickness of the periodic pattern. The amplitude ratio, β is computed by dividing the experimental film thickness amplitude by the Nusselt film thickness:

$$\beta = \frac{h_{max} - h_{min}}{2h^*}, \qquad [20]$$

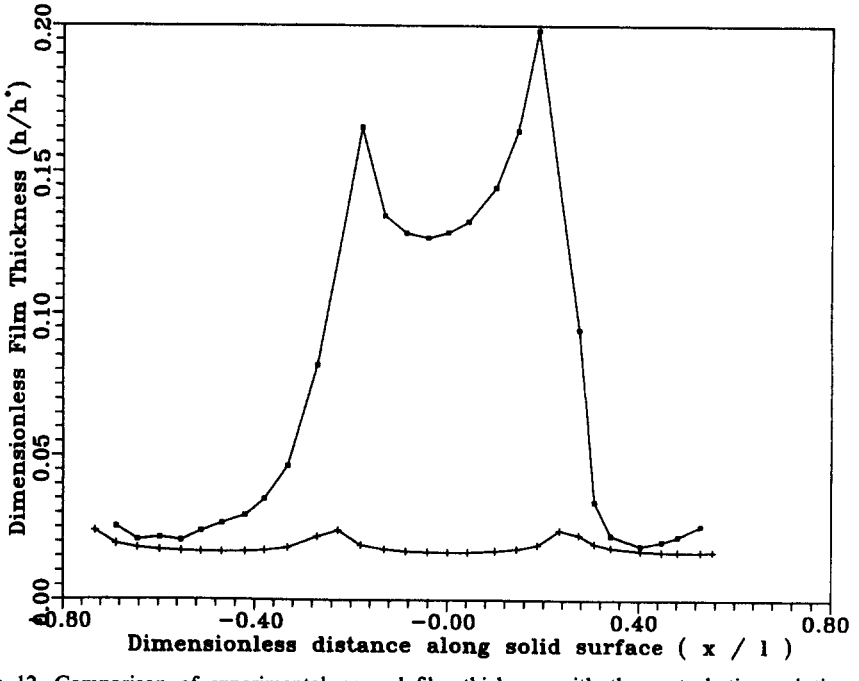

Figure 12. Comparison of experimental normal film thickness with the perturbation solution [14]; $a = 0.00635$ m, $h^* = 6.0 \times 10^{-4}$ m; ■, experimental +, theoretical.

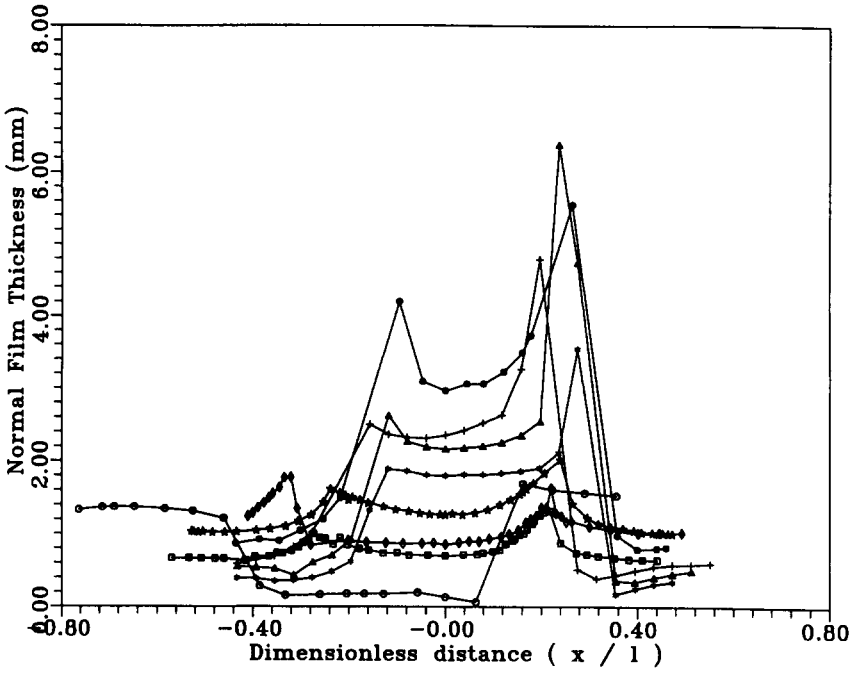

Figure 13. Effect of Nusselt film thickness on normal film thickness profiles δ: ○, 0.0836; □, 0.1078; ◇, 0.1482, ☆, 0.1575; ,0.1602; ▲, 0.2393; +, 0.2583; ●, 0.4724.

where h_{max} is the maximum film thickness of free surface position and h_{min} is the minimum film thickness or free surface position. The phase shift, ω, is the difference in degrees between the angular position of the minimum in the solid surface shape and the angular position of the minimum in the free surface position or film thickness:

$$\omega = \theta_{fs} - \theta_{ss}. \qquad [21]$$

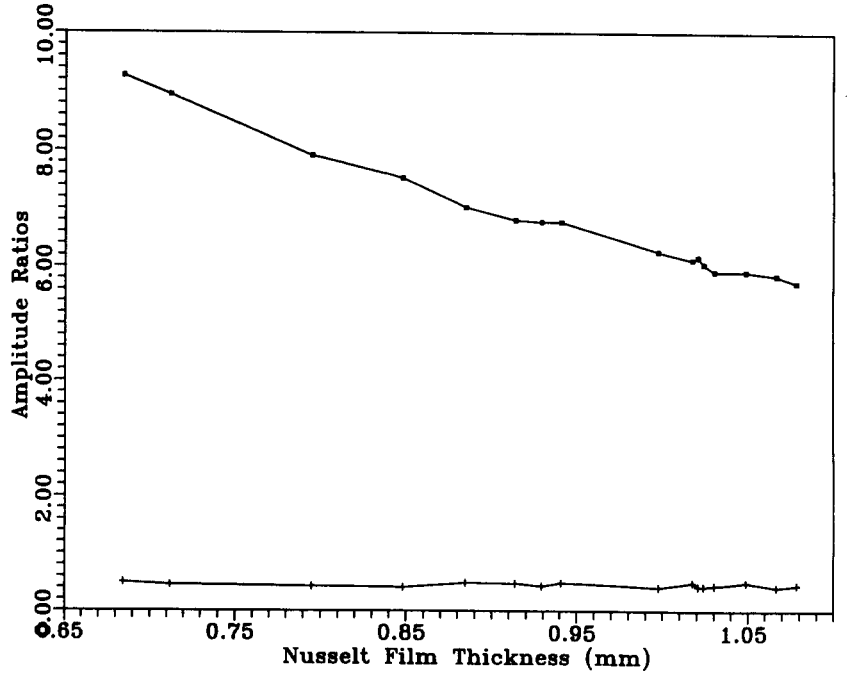

Figure 14. Experimental amplitude ratios; $a = 0.0254$ m: ■, based on a free surface; +, based on film thickness.

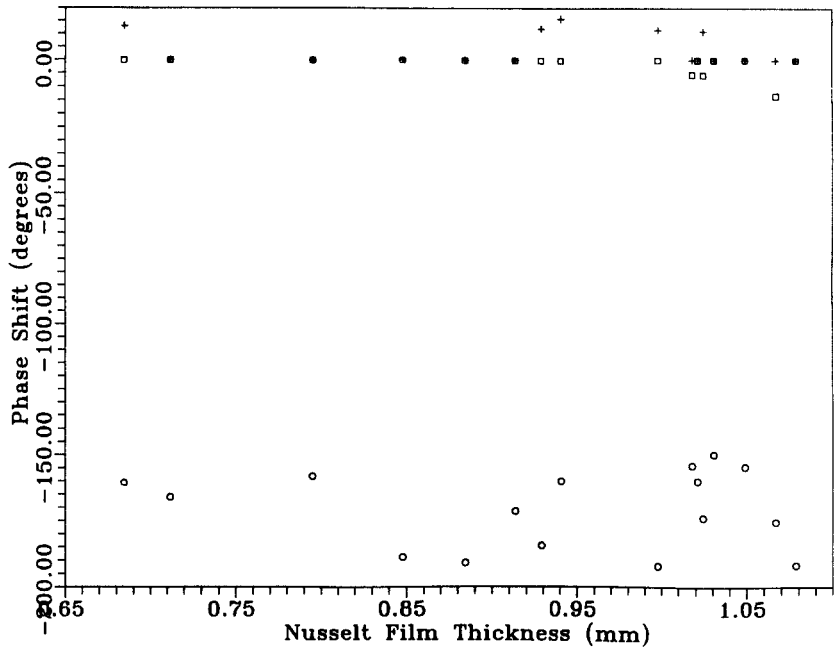

Figure 15. Experimental phase shift; $a = 0.0254$ m: □, based on a free surface; +, based on film thickness (upstream); ○, based on film thickness (downstream).

The phase shift and the amplitude of the free surface are relevant to the mass transfer processes. The phase shift and amplitude of the film thickness are relevant to film stability and dry patch formation. Figures 14 and 15 show the amplitude ratios and phase shifts as function of the Nusselt film thickness. Since the liquid film closely follows the contour of the solid surface, the amplitude ratio based on the free surface position is much higher than that based on the film thickness. It is interesting here to observe that for a periodic surface with a lower amplitude (Zhao & Cerro 1992), the amplitude ratio based on the film thickness was greater than that based on the free surface. It is observed that, whereas the amplitude ratio based on the free surface position decreased

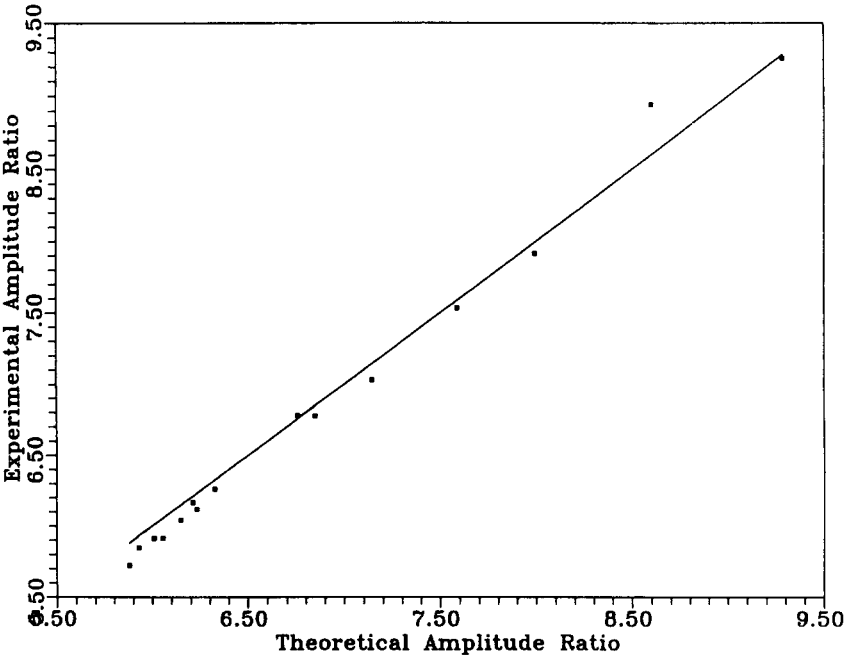

Figure 16. Parity plot of amplitude ratios based on free surface position; $a = 0.0254$ m.

linearly with an increase in the Nusselt film thickness, the amplitude ratio based on the film thickness remained relatively unchanged. This indicates that the free surface becomes flatter as the flow rate increases. Figure 15 shows that the solid surface minimum coincides with the position of the free surface minimum and a minimuim in the film thickness. The other minimum in film thickness lags the minimum solid surface position by nearly 180°. Figure 16 presents a parity plot of the experimental and theoretical (from low Re perturbation solution) values of the amplitude ratio based on the free surface position.

7. CONCLUDING REMARKS

A two-dimensional streamline function was used to derive the complete form of the film evolution equation for flow of a thin viscous film over a complex surface. It can be seen from the film evolution equation that except in cases of extremely high surface tension, inertial and capillary effects amount to an order ε contribution to the free surface profile, for small values of δ. Therefore, over the range of parameters studied in this work, there is a dynamic local equilibrium between gravity and viscous forces in the liquid film. The zero-order solution of this nonlinear ordinary differential equation is therefore similar to a sequence of quasi-steady-state Nusselt solutions for viscous film flow over a surface of continuously varying inclinations θ with respect to the vertical. The local values of θ are determined by the amplitude of the solid surface and by the local normal to the free surface. Agreement between experimental and theoretical normal film thickness is very good for small values of δ. When δ increases, either by increasing the flow rate or decreasing the solid surface amplitude, inertial and capillary effects cannot be neglected. Higher order solutions of [10] can be designed to include these effects.

Acknowledgements—This research was supported by Grant CTS-8912784 from the National Science Foundation, Division of Chemical and Thermal Systems, Fluid, Particulate & Hydraulic Systems Program. Support from the Office of Research and the Office of the Associate Dean for Research of the College of Engineering and Applied Sciences of The University of Tulsa is also gratefully acknowledged.

REFERENCES

DASSORI, C. G., DEIBER, J. A. & CASSANO, A. E. 1984 Slow two-phase flow through a sinusoidal channel. *Int. J. Multiphase Flow* **10,** 181–193.

FULFORD, G. D. 1964 The flow of liquids in thin films. *Adv. Chem. Engng* **5,** 151–236.

HIGGINS, B. G., SILLIMAN, W. J., BROWN, R. A. & SCRIVEN, L. E. 1977 Theory of meniscus shape in film flow. *Ind. Engng Chem. Fundam.* **16,** 393–401.

POZRIKIDIS, C. 1988 The flow of a liquid film along a periodic wall. *J. Fluid Mech.* **188,** 275–300.

DE SANTOS, J. M., MELLI, T. R. & SCRIVEN, L. E. 1991 Mechanics of gas–liquid flow in packed-bed contactors. *A. Rev. Fluid Mech.* **23,** 233–260.

WANG, C. Y. 1981 Liquid film flowing slowly down a wavy incline. *AIChE Jl* **27,** 207–212.

WHITTAKER, E. T. & WATSON, G. N. 1927 *A Course of Modern Analysis*, Chap. XX, 4th edn. Cambridge Univ. Press, London.

ZHAO, L. 1991 Liquid film flows over complex surfaces. Ph.D. Dissertation, University of Tulsa, OK.

ZHAO, L. & CERRO, R. L. 1992 Experimental characterization of viscous film flows over complex surfaces. *Int. J. Multiphase Flow* **18,** 495–516.